The Astrophysical Journal Letters, 882:L20 (8pp), 2019 September 10 https://doi.org/10.3847/2041-8213/ab3bd0

Thermal Evolution of Hydrated Asteroids Inferred from Oxygen Isotopes

Lionel G. Vacher[1,2], Maxime Piralla[1], Matthieu Gounelle[3], Martin Bizzarro[4], and Yves Marrocchi[1]
[1] CRPG, CNRS, Université de Lorraine, UMR 7358, Vandoeuvre les Nancy, F-54501, France; l.vacher@wustl.edu
[2] Department of Physics, Washington University, St. Louis, MO, USA
[3] IMPMC, MNHN, UPMC, UMR CNRS 7590, 61 rue Buffon, F-75005 Paris, France
[4] Centre for Star and Planet Formation and Natural History Museum of Denmark, University of Copenhagen, DK-1350 Copenhagen, Denmark
Received 2019 July 25; revised 2019 August 14; accepted 2019 August 15; published 2019 September 6

Abstract

Chondrites are fragments of unmelted asteroids that formed due to gravitational instabilities in turbulent regions of the Solar protoplanetary disk. Hydrated chondrites are common among meteorites, indicating that a substantial fraction of the rocky bodies that formed early in the solar system accreted water ice grains that subsequently melted due to heat released by the radioactive decay of ^{26}Al. However, the thermal histories of asteroids are still largely unknown; increased knowledge would provide fundamental information on their timing of accretion and their physical characteristics. Here we show that hydrated meteorites (CM chondrites) contain previously uncharacterized calcium carbonates with peculiar oxygen isotopic compositions ($\Delta^{17}O \approx -2.5‰$), which artificially produce the mass-independent trend previously reported for carbonates. Based on these isotopic data, we propose a new model to quantitatively estimate the precipitation temperatures of secondary phases (carbonates and serpentine). It reveals that chondritic secondary phases recorded a gradual increase in temperature during the extent of aqueous alteration, from −10°C to a maximum of 250°C. We also show that the thermal path of C-type asteroids is independent of the initial oxygen isotopic composition of the primordial water ice grains that they accreted. Our estimated temperatures for hydrated asteroids remain lower than those experienced by other carbonaceous chondrites, providing strong constraints for modeling the formation conditions and size distribution of water-rich asteroids, especially in anticipation of the return of samples of water-rich asteroids to Earth by the *OSIRIS-REx* and *Hayabusa2* missions.

Key words: meteorites, meteors, meteoroids – minor planets, asteroids: general – protoplanetary disks

1. Introduction

Dark C-type asteroids dominate the main-belt asteroid population and are genetically related to hydrous primitive CI and CM carbonaceous chondrites (Vilas & Gaffey 1989; Hiroi et al. 1996; Vilas 1994; Burbine et al. 2002; Lauretta et al. 2019). CM chondrites are the most common water-rich meteorites, and CM-like matter represent an important fraction of exogenic clasts reported in other groups of meteorites, implying that CM parent bodies are widespread in the asteroid belt (Briani et al. 2012). CM chondrites are complex aggregates of high-temperature components formed in the disk and low-temperature secondary minerals formed during subsequent parent-body fluid circulations. The latter provide key constraints on the origin of water accreted by asteroids (Vacher et al. 2016; Piani et al. 2018) as well as their accretion and evolution histories (Young et al. 2003; Fujiya et al. 2015; Vacher et al. 2017; Verdier-Paoletti et al. 2017). CM chondrites are therefore important samples because they show varying degrees of alteration that can be easily estimated by their chemical alteration index (Rubin et al. 2007; Marrocchi et al. 2014; Vacher et al. 2018). Among secondary minerals, carbonates are of primary importance as they represent direct proxies of the asteroidal fluids from which they formed and can, in theory, be used to decipher their thermal evolution (Clayton & Mayeda 1984). However, determining carbonate precipitation temperatures requires knowledge of the O isotopic compositions of their parental fluids, which itself requires knowledge of the carbonate precipitation temperatures, leading to a seemingly circular problem.

The temperature of CM carbonate precipitation remains largely underconstrained and proposed values cover a large range of temperatures. More generally, the sequence of formation of the different secondary phases (carbonates, serpentine) is poorly understood. Based on "clumped-isotopes" and oxygen isotopic analyses, it has been proposed that CM carbonates could have precipitated at both low and medium temperatures, in the range of 0°C–75°C (Clayton & Mayeda 1984; Benedix et al. 2003; Guo & Eiler 2007) and 50°C–350°C (Alexander et al. 2015; Verdier-Paoletti et al. 2017). However, these two different methodologies do not take into account the petrographic relationship between carbonates and serpentine (Fuchs et al. 1973; Zolensky et al. 1997; Brearley 2006; Rubin et al. 2007; Lee et al. 2013, 2014; Vacher et al. 2018), which can constrain the evolution of the fluid over time. In addition, different types of carbonates are present in CM chondrites (Lee et al. 2013, 2014; Vacher et al. 2017) but no specific attention has been paid on their respective oxygen isotopic compositions. The objectives of this Letter are thus to determine the oxygen isotopic composition of petrographically characterized carbonates in order to quantify the thermal evolution of hydrated asteroids. To do so, we surveyed a suite of different CM chondrites characterized by varying degrees of alteration: CM2.6/2.7 Maribo (van Kooten et al. 2018), CM2.5 Murchison (Rubin et al. 2007), CM2.4/2.7 Jbilet Winselwan (King et al. 2018), and CM2.0 Mukundpura (Rudraswami et al. 2018). Based on oxygen isotopic compositions of carbonates, we propose a new isotopic alteration model that reconciles petrographic observations and formation temperatures of CM carbonates.

2. Material and Methods

2.1. Scanning Electron Microscope (SEM) Imaging

Calcite grains were located in carbon-coated (i) polished sections of Murchison, Mukundpura, and Jbilet Winselwan (samples provided by the Muséum National d'Histoire Naturelle in Paris) and (ii) thin section of Maribo (section

provided by the Natural History Museum of Denmark in Copenhagen) using a SEM JEOL JSM-6510 equipped with an energy dispersive X-ray detector (Bruker-AXS XFlash, silicon drift detector) at Centre de Recherches Pétrographiques et Géochimiques (CRPG; Nancy, France). Back-scattered electron (BSE) imaging were performed with a 3 nA electron beam current operated at 15 kV.

2.2. Oxygen Isotope Analyses of Calcite

Calcite oxygen isotopic compositions were analyzed using a CAMECA IMS 1270 E7 at CRPG laboratory. A Cs+ primary ion beam (~15 × 10 μm spot area) with a current of ~5 nA was used in order to collect $^{16}O^-$, $^{17}O^-$ and $^{18}O^-$ secondary ions in multi-collection mode using three Faraday cups (L'2, FC2, and H1). Charge compensation was applied using a normal-incidence electron gun. Mass resolving power (MRP = $M/\Delta M$) was adjusted to ~7000 to resolve interference from $^{16}OH^-$ on the $^{17}O^-$ peak and achieve maximum flatness on the top of the $^{16}O^-$ and $^{18}O^-$ peaks (entrance and exit slits of FC2 were adjusted to ~70 μm and ~170 μm, respectively). $^{16}O^-$ and $^{18}O^-$ secondary ions were collected on L'2 and H1, respectively (slit 1, MRP ≈ 2500). Pre-sputter on a large area (~20 × 20 μm) was applied before each measurement during 60 s in order to remove the carbon coating at the surface of the calcite grains. Acquisition time was set to ~5 s and measurements were repeated over 30 cycles to achieve counting statistics ~0.2‰ (1σ) for $\delta^{18}O$ and ~0.3‰ for $\delta^{17}O$. Isotope ratios ($^{17}O/^{16}O$ and $^{18}O/^{16}O$) are presented in per mil (‰) relative to standard mean ocean water (SMOW):

$$\delta^{x}O_{SMOW}(‰) = \left(\frac{{}^{x}O/{}^{16}O_{sample}}{{}^{x}O/{}^{16}O_{SMOW}} - 1\right) \times 1000 \qquad (1)$$

where x represents ^{17}O or ^{18}O and SMOW the ratios of the SMOW standard. We measured two in-house terrestrial standards to define the Terrestrial Fractionation Line (TFL): (i) quartz (SiO_2) from Brazil ($\delta^{18}O$ = 9.6‰, $^{16}O = 2 \times 10^9$ cps and $^{18}O = 4.2 \times 10^6$ cps) and (ii) calcite ($CaCO_3$) from Mexico ($\delta^{18}O$ = 23.6‰, $^{16}O = 2 \times 10^9$ cps and $^{18}O = 4.2 \times 10^6$ cps; 0.03 wt% of MgO). The instrumental mass fractionation (IMF) for calcite matrix was determined from our in-house Mexican calcite standard at the beginning and end of each analytical session. IMF values for each sample analysis were then calculated by accounting for the linear deviation over the time of the IMF values. Typical measurement errors (2σ), accounting for errors on each measurement and the external reproducibility of the standard, were estimated to be ~0.5‰ for $\delta^{18}O$, ~0.6‰ for $\delta^{17}O$, and ~0.7‰ for $\Delta^{17}O$ (i.e., $\Delta^{17}O = \delta^{17}O - 0.52 \times \delta^{18}O$), where $\Delta^{17}O$ represents the departure from the TFL.

3. Results

In the four CM chondrites surveyed in this work (Table 1), calcite grains surrounded by Fe–S-rich serpentine/tochilinite (hereafter T1 calcite; Figure 1(a)) are ubiquitous, whereas serpentine-free polycrystalline calcite grains containing Fe–Ni sulfide inclusions (hereafter T2 calcite; Figure 1(b)) have only been observed in two sections (Jbilet Winselwan and Mukundpura). The O isotopic compositions of T1 calcite grains measured herein vary widely, with $\delta^{18}O$ values ranging from 23.1 to 44.3‰, $\delta^{17}O$ from 11.1 to 23.4‰ and $\Delta^{17}O$ from −2.8 to +1.8‰ (Figures 1(c) and 5, Table 2), whereas T2 calcite grains have homogeneous compositions with $\delta^{18}O$ values ranging from 12.6 to 18.4‰, $\delta^{17}O$ from 4.2 to 8.1‰ and $\Delta^{17}O$ from −4 to −0.8‰ (Figures 1(c) and 5, Table 3).

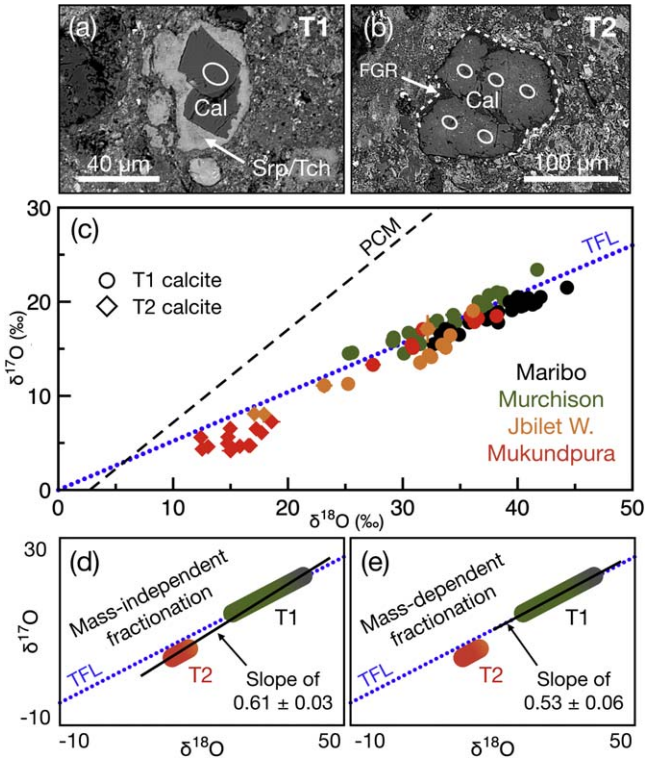

Figure 1. BSE images of (a) a T1 calcite grain (Cal) surrounded by a Fe–S-rich serpentine/tochilinite rim (Srp/Tch) in the matrix of Murchison and (b) a T2 calcite grain that is free of serpentine/tochilinite rim, but is instead surrounded by a rim of fine-grained matrix (FGR; white dashed line) in the matrix of Mukundpura. White circles represent the locations of SIMS analytical spots. (c) $\delta^{17}O$–$\delta^{18}O$ plot for T1 (circles) and T2 (diamonds) calcites from the CM chondrites Maribo (black), Murchison (green), Jbilet Winselwan (orange), and Mukundpura (red; 2σ errors). Schematic $\delta^{17}O$–$\delta^{18}O$ diagrams represent the linear correlations (black solid lines) obtained considering (d) T1 and T2 calcites, defining a mass-independent trend with a slope of 0.61 ± 0.03 and (e) only T1 calcites, defining a mass-dependent trend with a slope of 0.53 ± 0.06. TFL = ($\delta^{17}O = 0.52 \times \delta^{18}O$); primary chondrule minerals (PCM) line = ($\delta^{17}O = 0.987 \times \delta^{18}O$–2.7).

4. Discussion

Together, T1 and T2 calcite grains define a mass-independent trend with $\delta^{17}O = (0.61 \pm 0.03) \times \delta^{18}O$–(3.3 ±1.1) (Figures 1(c)–(d)) that is similar, within errors, to those commonly reported in different CM chondrites (Vacher et al. 2018). As a first approximation, this trend suggests that the O isotopic compositions of CM carbonates is essentially controlled by variable degrees of isotopic exchanges between ^{16}O-rich anhydrous silicates and a $^{17,18}O$-rich fluid (Figure 1(d); Verdier-Paoletti et al. 2017; Marrocchi et al. 2018). However, the O isotopic compositions of T1 calcites alone define a distinct trend with $\delta^{17}O = (0.53 \pm 0.06) \times \delta^{18}O$–(1.2 ± 2.2) that is indistinguishable, within errors, from the TFL (i.e., $\Delta^{17}O = -0.4 \pm 1.0$; Figure 1(e)). Conversely, T2 calcites exhibit clustered $\delta^{17}O$–$\delta^{18}O$ values (Figures 1(c) and 5, Table 3) with $\Delta^{17}O = -2.6 \pm 1.0$, which artificially produce the aforementioned mass-independent trend when taken together with T1 calcites (Figure 1(d)). This demonstrates that petrographic

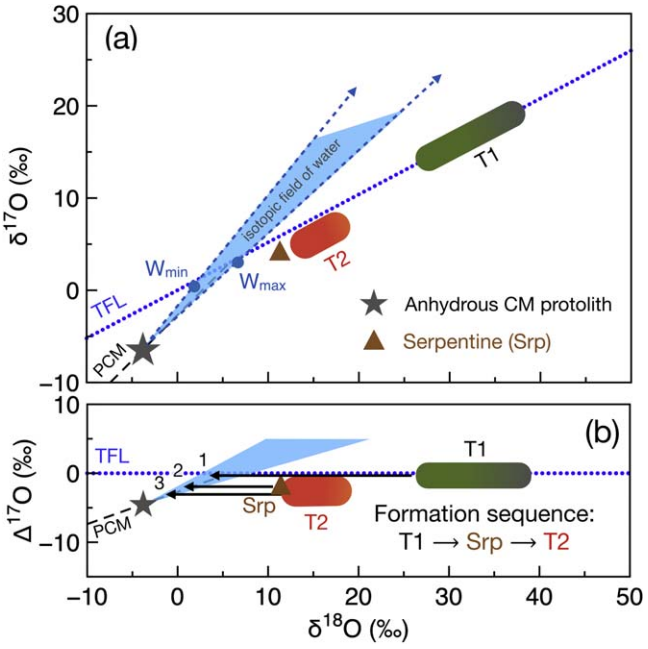

Figure 2. (a) $\delta^{17}O$–$\delta^{18}O$ plot showing simplified ranges for T1 and T2 calcites, the mean bulk value of CM serpentine (Srp, brown triangle) and the isotopic field of CM water (blue shaded area) as determined from the isotopic equilibration (blue dashed lines) of the minimum (W_{min}) and maximum (W_{max}) compositions of the parental water of T1 calcites (blue circles) with the anhydrous CM protolith (gray star; see Figure 5 for details). (b) $\delta^{18}O$–$\Delta^{17}O$ plot showing the isotopic equilibration of CM water with the anhydrous CM protolith. In this diagram, mass-dependent isotopic fractionations plot on a horizontal line. The decrease of the mean $\Delta^{17}O$ values of the secondary phases ($\Delta^{17}O_{T1} = 0.4‰$, $\Delta^{17}O_{Srp} = -2.2‰$ and $\Delta^{17}O_{T2} = -2.4‰$; see Tables 2 and 3 and Clayton & Mayeda 1999) indicates the following formation sequence: (1) T1 calcites, (2) serpentines, and (3) T2 calcites.

observations of carbonates are essential for understanding the O isotopic evolution of asteroidal fluids and the constraints that they bear.

Based on mass-balance calculations, tentative attempts at estimating the O isotopic composition of primordial water accreted by CM chondrites have led to widely ranging and contrasted results due to assumptions on the O isotopic composition of the anhydrous protolith and asteroidal thermal evolution ($\delta^{18}O_{fluid} = 16$–$55‰$, $\delta^{17}O_{fluid} = 9$–$35‰$ and $\Delta^{17}O_{fluid} = 0.9$–$6.6‰$; Clayton & Mayeda 1999; Verdier-Paoletti et al. 2017; Fujiya 2018). However, these values correspond to the initial water composition and do not represent the oxygen isotopic compositions of fluids from which carbonates precipitated, which had Earth-like compositions with $\Delta^{17}O \approx 0‰$ (Figure 1(c); Vacher et al. 2016; Verdier-Paoletti et al. 2017). Quantitative estimates of the O isotopic compositions of the parental fluids of carbonates have been obtained by CO_2 clumped-isotope thermometry (Δ^{47}; Guo & Eiler 2007), which corresponds to anomalous enrichments of mass 47 (i.e., $^{13}C^{18}O^{16}O$) in CO_2 derived from H_3PO_4 digestion of carbonates (Ghosh et al. 2006). Based on measurements performed on the CM chondrites Murchison and Murray, dominated by T1 calcites, Guo & Eiler (2007) estimated that the O isotopic compositions of their alteration fluids ranged from $\delta^{18}O = 2‰$ and $\Delta^{17}O = -0.6‰$ (hereafter W_{min}; Figure 2(a)) to $\delta^{18}O = 6.8‰$ and $\Delta^{17}O = -0.5‰$ (hereafter W_{max}; Figure 2(a)). Because these fluids experienced oxygen isotopic exchanges with the anhydrous CM chondrite protolith ($\delta^{18}O = -3.8‰$, $\delta^{17}O = -6.5‰$; Figure 6), they define two trends that delimit the possible O isotopic compositions of CM alteration fluids (blue shaded area in Figure 2(a)). Considering these extreme trends, the precipitation temperatures of each T1 calcite grain can be calculated according to the isotopic fractionation factor α (Watkins et al. 2013), which corresponds to the distance between the minimum and maximum trends and the O isotopic compositions of carbonates in the three oxygen isotope diagram. This estimation leads to respective minimum (T_{min}) and maximum (T_{max}) precipitation temperatures of -9 ± 11°C and 5 ± 14°C for Maribo, 19 ± 22°C and 50 ± 34°C for Murchison, 15 ± 21°C and 33 ± 29°C for Jbilet Winselwan, and 12 ± 17°C and 34 ± 22°C for Mukundpura (1σ; Table 1 and Figure 3(a)). On average, this gives minimum and maximum precipitation temperatures for all T1 calcites of 7 ± 22°C and 29 ± 32°C, respectively (1σ).

The large range of $\delta^{17}O$–$\delta^{18}O$ values and constant $\Delta^{17}O$ values observed in T1 calcites (Figures 1(c)–(e), Table 2) imply that T1 calcites precipitated along a temperature gradient from alteration fluids characterized by a fixed $\Delta^{17}O$ value. On the other hand, T2 calcites (this study) and serpentine (Clayton & Mayeda 1984) formed from a more ^{16}O-rich fluid that resulted from protracted isotopic exchange with the ^{16}O-rich anhydrous protolith and thus evolved toward negative $\Delta^{17}O$ values (Figure 2(b)). Following the same methodology as for T1 calcites, we calculated the formation temperatures of T2 calcites to be significantly higher, with respective minimum and maximum temperatures being 109 ± 11°C and 158 ± 22°C for Jbilet Winselwan and 110 ± 11°C and 139 ± 55°C for Mukundpura (1σ; Table 1 and Figure 3(a)); respective average values are 109 ± 29°C and 141°C ± 52°C (1σ). The same calculation for bulk serpentine compositions ($n = 5$; Clayton & Mayeda 1999) gives minimum and maximum formation temperatures of 28 ± 8 to 56 ± 13°C and 73 ± 7 to 98 ± 11°C, respectively, depending of the fractionation factor considered (Zheng 1993; Früh-Green et al. 1996; 1σ; Table 1, Figure 3(a), and Figure 4).

Our petrographic and isotopic approaches reveal that T1 calcites precipitated at lower temperatures than serpentines and T2 calcites (Figure 3(a)). These results support petrographic observations suggesting that T2 calcites correspond to a later stage of alteration, as highlighted by (i) the absence of serpentine rims and (ii) the existence of an FGR, suggesting that they replaced chondrule silicates (Figure 3(b); Lee et al. 2014; Lindgren et al. 2017). This implies that fluid circulation in CM parent bodies, and thus the formation of CM secondary phases, occurred during a prograde thermal evolution (Figures 2(b) and 3(b); Vacher et al. 2019), with T1 calcites forming first at $T = -10$ to $+50$°C, followed by the precipitation of (Fe,S)-rich serpentine (mostly cronstedtite; Pignatelli et al. 2016, 2017) and tochilinite at $T = 30$°C–100°C, and finally T2 calcites at $T = 110$°C–160°C (Figure 3(a), Table 1).

According to X-ray diffraction studies (Howard et al. 2011, 2009), serpentine represent the most abundant mineral in CM chondrites (75 vol% on average). Their formations (posterior to that of T1 calcites) would thus affect the isotopic

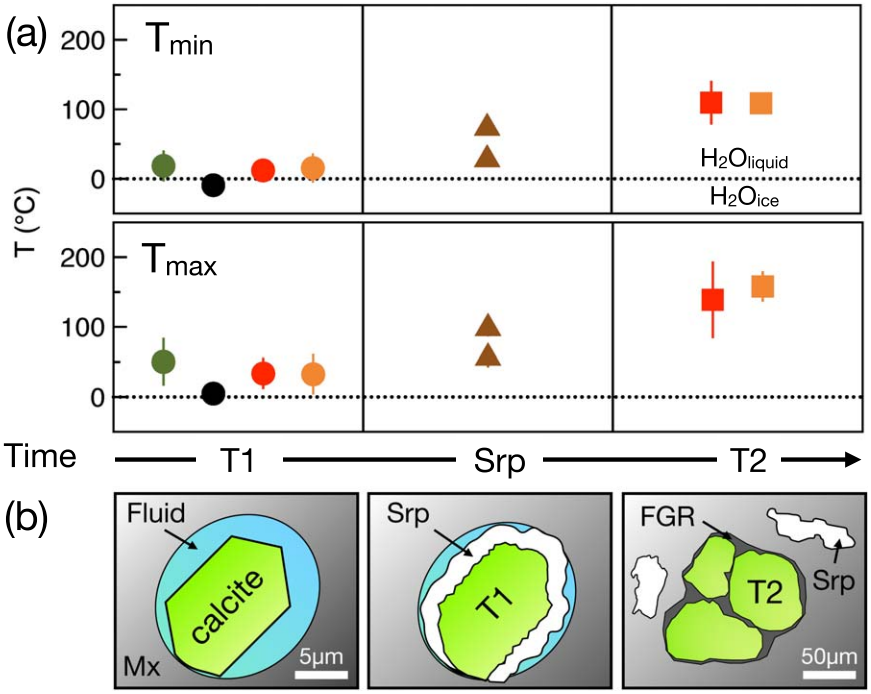

Figure 3. (a) Minimum (T_{min}) and maximum (T_{max}) precipitation temperatures of T1 calcites (circles), serpentines (brown triangles), and T2 calcites (diamonds) calculated as a function of their formation sequence/time (errors are 1σ) using previously reported fractionation factors for calcite (O'Neil et al. 1969) and serpentine (Zheng 1993; Früh-Green et al. 1996). Colors are the same as in Figure 1. (b) Schematic representation of the formation sequence of (1) T1 calcite, (2) serpentine around T1 calcite, and (3) T2 calcite, as deduced from petrographic observations and the mean $\Delta^{17}O$ values of these three phases (see Figure 2(c)).

Table 1
Mean O Isotopic Compositions of Secondary Phases and Their Calculated Minimum (T_{min}) and Maximum (T_{max}) Formation Temperatures (O'Neil et al. 1969); Uncertainties are 1σ

Meteorite	Petrologic Subtype	Secondary Phase	Sample Number	Mean $\delta^{18}O$ (‰)	Mean $\Delta^{17}O$ (‰)	Mean Tmin (°C)	Mean Tmax (°C)
Maribo	CM2.6/2.7 (a)	T1 calcite	25	38.3 *(±3.1)*	−1.2 *(±0.5)*	−9 *(±11)*	5 *(±14)*
Murchison	CM2.5 (b)	T1 calcite	24	33.7 *(±4.5)*	0.4 *(±0.8)*	19 *(±22)*	50 *(±34)*
Jbilet Winselwan	CM2.4/2.7 (c)	T1 calcite	10	31.4 *(±4.1)*	−1.6 *(±1.2)*	15 *(±21)*	33 *(±29)*
		T2 calcite	2	17.5 *(±0.6)*	−1 *(±0.3)*	109 *(±11)*	158 *(±22)*
Mukundpura	CM2.0 (d)	T1 calcite	8	33.5 *(±3.8)*	−0.7 *(±0.6)*	12 *(±17)*	34 *(±22)*
		T2 calcite	13	15.4 *(±2)*	−2.6 *(±1)*	110 *(±32)*	139 *(±55)*
Bulk CM	···	Serpentine (e)	5	11.7 *(±0.6)*	−2.2 *(±0.3)*	28 *(±8)* (f)	56 *(±13)* (f)
						73 *(±7)* (g)	98 *(±11)* (g)

References. (a) van Kooten et al. 2018. (b) Rubin et al. 2007. (c) King et al. 2018. (d) Rudraswami et al. 2018. (e) Clayton & Mayeda 1999. (f) Früh-Green et al. 1996. (g) Zheng 1993.

evolution of the alteration fluids, leading to a slight shift toward ^{16}O-enriched values. As this isotopic shift is not taken into account in our model, this implies that the precipitation temperatures estimated for T2 calcites (Figure 3(a), Table 1) should be considered as maximum values. However, as the fractionation factor α is significantly lower for serpentine-water than for calcite-water (i.e., $1000\ln\alpha_{serpentine\text{-}water} = 6.3$ versus $1000\ln\alpha_{calcite\text{-}water} = 17.1$ at 100°C; O'Neil et al. 1969; Früh-Green et al. 1996), this approximation does not affect our main conclusions that T1 calcites precipitated at lower temperature than T2 calcites.

As the uncertainties on the O isotopic compositions of primordial water accreted by CM chondrites could also affect our conclusions, we tested our results with different initial O isotopic compositions (Figure 4). According to the currently favored self-shielding model, primordial water is hypothesized to have had a large $^{17,18}O$ enrichment (i.e., $\delta^{17}O = \delta^{18}O \approx 180‰$; Sakamoto et al. 2007) plotting on a line of slope 1 in a three oxygen isotope diagram. However, mass-balance calculations performed on the O isotopic compositions of CM chondrites at bulk and mineral scales suggest more modest enrichments in the heavy oxygen isotopes with $\delta^{17}O = 35 \pm 9‰$ and $\delta^{18}O = 55 \pm 13‰$ (Fujiya 2018). Hence, we tested our results by using primordial CM water O isotopic compositions corresponding to (i) a composition intermediate between W_{min} and W_{max} (W_{int}) and (ii) the values proposed by

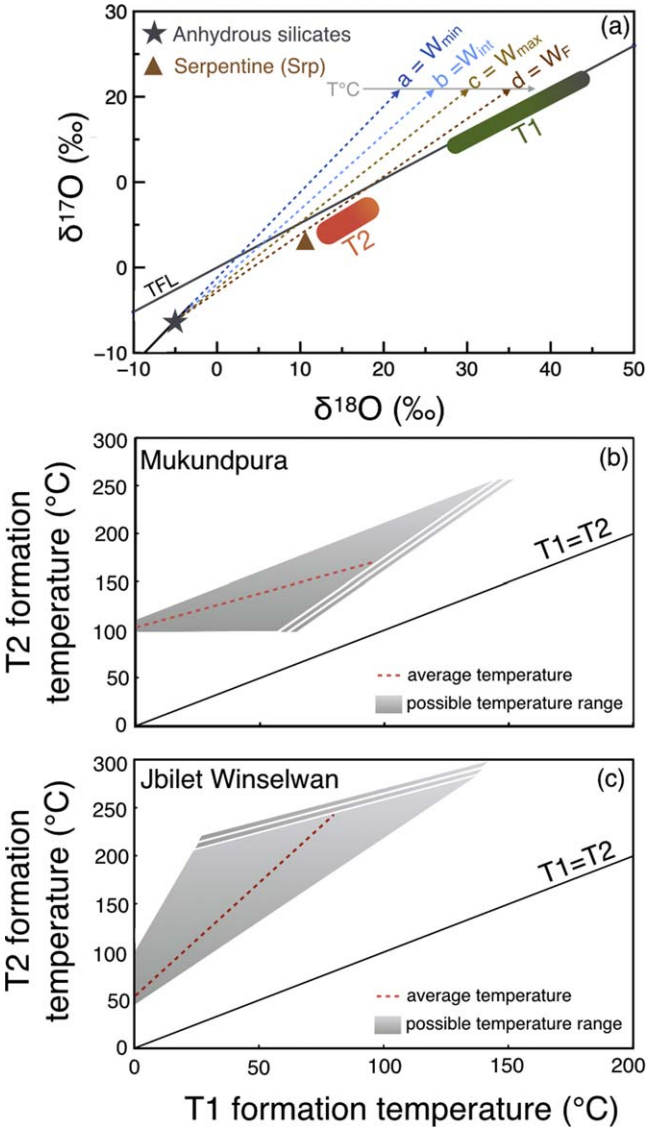

Figure 4. (a) $\delta^{17}O$–$\delta^{18}O$ plot showing the four trends (see the text) used to calculate the influence of the initial oxygen isotopic composition of primordial water on the thermal path interpreted for water-rich asteroids. (b), (c) $\delta^{17}O$–$\delta^{18}O$ plots showing the results of the model for Mukundpura and Jbilet Winselwan, respectively. In both cases, the average formation temperatures of T2 calcites are systematically higher than those estimated for T1 calcites (red dashed lines), even when accounting for variability in the $\delta^{17}O$ and $\delta^{18}O$ values of calcites in Jbilet Winselwan and Mukundpura (gray triangles).

Fujiya (2018; W_F, Figure 4(a)). Isotopic exchange between these fluid compositions and the anhydrous CM protolith (Marrocchi et al. 2018) thus defines two other lines on the $\delta^{17,18}O$ diagram (b and d in Figure 4(a), with lines a and c corresponding to the trends defined by W_{min} and W_{max}, respectively) from which the precipitation temperatures of T1 and T2 calcites can be calculated according to the fractionation factor α (Watkins et al. 2013). The results for Jbilet Winselwan and Mukundpura (the only meteorites containing T2 calcites in this study) systematically show that T2 calcites precipitated at higher temperatures than T1 calcites (Figures 4(b)–(c)), regardless of the oxygen isotopic composition used for primordial water. Depending on the isotopic trend considered (a, b, c, or d in Figure 4(a)), the average precipitation temperatures of T1 calcites range from 10°C to 100°C, whereas T2 calcites formed between 110°C and 245°C (Figures 4(b)–(c)). We note that the absolute temperatures at which secondary phases formed is directly affected by the oxygen isotopic composition of primordial chondritic water, whose precise determination is thus fundamental to better quantifying the thermal evolution of hydrated asteroids.

Another possible source of uncertainty in estimating precipitation temperatures arises if T1 calcites experienced post-precipitation isotopic re-equilibration, especially if CM chondrites experienced peak temperatures as high as 250°C. However, this appears unlikely as T1 calcites systematically show mass-dependent oxygen isotopic variations (Figure 7), whereas isotopic exchange between initial water and anhydrous silicates during re-equilibration would have induced $\Delta^{17}O$ variations (Figure 2(a)). In addition, according to the values of oxygen self-diffusion in calcite (Farver 1994; Anderson 1969), 1–10^4 Gyr are required to isotopically re-equilibrate calcite grains of 5 μm in size at temperatures $\leqslant$200°C (Figure 7). Such results thus strengthen our conclusion that hydrated asteroids experienced a prograde thermal evolution with T1 calcites precipitating first, followed by serpentine and then T2 calcites.

By taking into account the petrographic type of carbonates, our hydrothermal temperature estimates for CM chondrites are higher than previously proposed (Clayton & Mayeda 1984; Benedix et al. 2003; Guo & Eiler 2007) but remain low (<250°C) compared to the peak of thermal metamorphism experienced by other groups of carbonaceous chondrites, such as CO or CV chondrites (up to 500°C–600°C; Bonal et al. 2007; Busemann et al. 2007; Cody et al. 2008; Ganino & Libourel 2017). This implies the relatively late accretion of water-rich asteroids in the protoplanetary disk, as water-poor asteroids that accreted earlier experienced significantly higher temperatures due to the radioactive decay of ^{26}Al. Based on $\varepsilon^{54}Cr$ anomalies, it has been proposed than CM chondrites accreted ~3.7–5.0 Myr after the formation of CV calcium-aluminum-rich inclusions (CAIs; Fujiya et al. 2012; Sugiura & Fujiya 2014; Doyle et al. 2015), after a five-fold decrease in the abundance of ^{26}Al, whereas CO and CV chondrites accreted ~2.1–2.4 and ~2.4–2.6 Myr after CV CAIs, respectively (Doyle et al. 2015). Interestingly, recent spectral data provided by the *Osiris-REx* and *Hayabusa2* asteroid sample return missions suggest that C-type asteroid Ryugu has experienced more heating than B-type asteroid Bennu (Hamilton et al. 2019; Kitazato et al. 2019). Although late shock heating could have induced such features, their different thermal history could also be the result of distinct accretion ages. The returned samples from *Osiris-REx* and *Hayabusa2* in the near future will likely contain hydrated minerals (Kitazato et al. 2019; Lauretta et al. 2019) whose in-situ isotopic analyses could provide information on the thermal alteration processes and formation histories of asteroids Ryugu and Bennu.

5. Conclusions

In this Letter, we report the results of in-situ oxygen isotope analyses performed on alteration phases (calcium carbonates) from a suite of different hydrated meteorites (CM chondrites) to quantitatively estimate the thermal evolution of hydrated asteroids. Based on our isotopic results, we propose a new isotopic model that reconciles formation temperatures and petrographic observations of secondary minerals whose isotopic compositions recorded a gradual increase of the

temperature (up to 250°C) during a prograde evolution of the temperature, regardless the oxygen isotopic composition of the initial water. These results are fundamental because they imply that hydrated asteroids accreted relatively late in the protoplanetary disk, as their earlier accretion would have led to higher alteration temperatures due to higher concentrations of radioactive ^{26}Al. Although more precise radioactive dating and numerical modeling are required, our study provides a key method to quantitatively estimate the respective thermal histories of the asteroids Bennu (Lauretta et al. 2019) and Ryugu (Sugita et al. 2019; Watanabe et al. 2019) upon the return of samples to Earth.

The authors are grateful to Nordine Bouden and Johan Villeneuve for their assistance with the isotopic measurements. Laurette Piani is thanked for helpful scientific discussions. The Muséum National d'Histoire Naturelle (Paris) and The Natural History Museum of Denmark (Copenhagen) are also thanked for providing samples of Mukundpura and sections of Maribo chondrites. We thank Prof. Frederic Rasio for his editorial handling and the anonymous reviewer for comments that contributed to improve the quality of the manuscript. This research was funded by l'Agence Nationale de la Recherche through grant ANR-587 14-CE33-0002-01 SAPINS (PI Yves Marrocchi). This is CRPG contribution #2714.

Appendix

This Appendix shows (i) the oxygen isotopic composition of carbonates in the different chondrites selected for this study, (ii) the bulk oxygen isotopic compositions used to calculate the primordial isotopic composition of the anhydrous protolith, and (iii) the time required for the complete re-equilibration of calcites (Clayton & Mayeda 1999; Hewins et al. 2014; Ushikubo et al. 2012; Petitat et al. 2011; Fujiya et al. 2012; Doyle et al. 2015; Farver 1994).

Table 2
Oxygen Isotopic Compositions of T1 Calcite Grains in the CM Chondrites Maribo, Murchison, Jbilet Winselwan, and Mukundpura

#	δ^{18}O	2σ	δ^{17}O	2σ	Δ^{17}O	2σ
CC7	32.7	0.3	15.5	0.5	−1.5	0.8
CC21-1	33.3	0.3	16.5	0.8	−0.8	1
CC21-2	33.9	0.3	16.3	0.7	−1.3	0.9
CC22	33.7	0.3	17.1	0.5	−0.4	0.8
CC20	34.1	0.4	16.9	0.6	−0.9	0.9
CC27	34.9	0.2	16.5	0.5	−1.7	0.7
CC30	35.8	0.3	17.8	0.5	−0.8	0.7
CC10	37.3	0.6	18.1	0.6	−1.3	1
CC11	37.7	0.2	18.4	0.5	−1.3	0.7
CC4-2	38	0.3	18.6	0.5	−1.1	0.8
CC4-1	41.6	0.3	19.9	0.5	−1.7	0.7
CC5	38.3	0.3	18.9	0.6	−1.1	0.8
CC17	38.3	0.3	17.8	0.6	−2.2	0.8
CC9	39.3	0.3	20	0.5	−0.4	0.8
CC33	39.5	0.3	19.1	0.5	−1.4	0.5
CC32	39.5	0.3	19.6	0.7	−0.9	0.9
CC13	40	0.5	20.5	0.6	−0.3	1
CC3	40.2	0.3	20	0.6	−0.9	0.7
CC28	40.3	0.2	19.5	0.6	−1.4	0.8
CC29	40.5	0.3	19.6	0.6	−1.5	0.6
CC12	40.6	0.3	19.7	0.5	−1.4	0.8
CC15	40.9	0.4	20.4	0.5	−0.9	0.6
CC2	41.3	0.3	19.7	0.5	−1.7	0.8
CC18	42	0.3	20.5	0.5	−1.4	0.8
CC1	44.3	0.3	21.5	0.6	−1.5	0.8
Mean	38.3		18.7		−1.2	
StDev	*3.1*		*1.6*		*0.5*	
CC-7-2	25.3	0.2	14.5	0.4	1.3	0.3
CC-7-3	25.6	0.2	14.6	0.4	1.3	0.4
A-CC-5-2	29.1	0.5	15.8	0.4	0.7	0.6
A-CC-5-3	36.6	0.2	20	0.3	1	0.3
A-CC-8-2	29.2	0.6	15.9	0.6	0.7	0.7
CC-1-2	29.2	0.3	16.2	0.4	1	0.4
A-CC-11-1	30.1	0.5	14.5	0.6	−1.1	0.7
CC-6	30.5	0.3	16.7	0.3	0.8	0.4
A-CC-3-2	31.3	0.9	16.5	0.8	0.3	1.1
A-CC-3-1	34.4	0.7	18.6	0.7	0.7	0.9
A-CC-10	31.5	0.9	15.5	0.6	−0.9	1.0
A-CC-13	32.6	0.3	17.6	0.3	0.7	0.4
A-CC-7	33	0.5	17.1	0.6	0	0.7
CC-18	33	0.2	18	0.3	0.9	0.3
A-CC-2-2	34.4	0.6	17.6	0.6	−0.3	0.8
CC-3	34.6	0.3	17.8	0.4	−0.2	0.4
CC-2	36.8	0.2	19	0.3	−0.1	0.3
CC-5	37.3	0.6	19.4	0.6	0	0.8
CC-10	37.5	0.2	20.7	0.3	1.2	0.3
CC-12	38.2	0.3	21	0.3	1.1	0.3
A-CC-1	38.6	0.6	20.9	0.6	0.8	0.8
CC-11	38.8	0.3	20.2	0.3	0	0.4
CC-9	40.3	0.3	20.1	0.3	−0.8	0.4
CC-8	41.7	0.4	23.4	0.3	1.8	0.4
Mean	33.7		18		0.4	
StDev	*4.5*		*2.4*		*0.8*	
CC-6	23.1	0.7	11.1	0.8	−0.9	1.0
CC-5	25.2	0.4	11.3	0.7	−1.9	0.7
CC-11	31.5	0.5	13.5	0.8	−2.8	0.9
CC-3	32.2	0.7	17.1	1.5	0.4	1.6
CC-2	32.3	0.6	14.3	0.7	−2.4	0.8
CC-7	32.5	0.5	14.1	0.7	−2.8	0.7
CC-9	33.4	0.5	15.4	0.7	−1.9	0.7
CC-8	33.7	0.5	15.1	0.8	−2.4	0.8
CC-1	34.1	0.5	16.4	0.7	−1.3	0.8
CC-10	36.1	0.5	19.1	0.8	0.3	0.8
Mean	31.4		14.8		−1.6	
StDev	*4.1*		*2.5*		*1.2*	
CC15	27.4	0.7	13.3	0.4	−0.9	0.6
CC13	30.8	0.6	15.4	0.4	−0.6	0.6
CC14	30.9	0.6	15.1	0.4	−1	0.6
CC1	31.8	0.5	17.1	0.4	0.6	0.5
CC12	35.9	0.6	18.5	0.4	−0.2	0.6
CC8-1	36.2	0.6	17.8	0.4	−1	0.6
CC11	36.5	0.6	18.2	0.4	−0.8	0.6
CC7-1	38.2	0.6	18.5	0.4	−1.4	0.6
Mean	33.5		16.7		−0.7	
StDev	*3.8*		*1.9*		*0.6*	

Note. Shaded rows denote multiple analyses of the same grain.

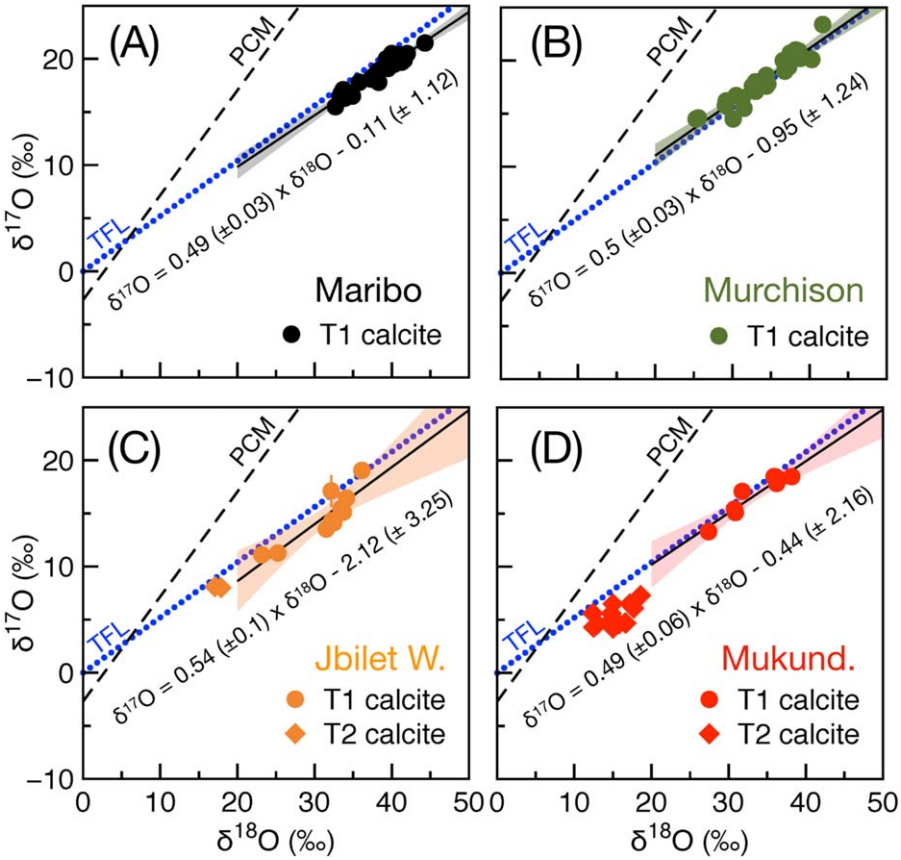

Figure 5. $\delta^{17}O$–$\delta^{18}O$ plots showing the mass-dependent trends (black solid line) defined by T1 calcites (circles) for each CM chondrite: (a) Maribo, (b) Murchison, (c) Jbilet Winselwan, and (d) Mukundpura. Shaded areas represent the 95% confidence interval for each slope. T2 calcites (diamonds) are also shown for Jbilet Winselwan (c) and Mukundpura (d), the only chondrites studied herein containing T2 calcites. Errors are 2σ.

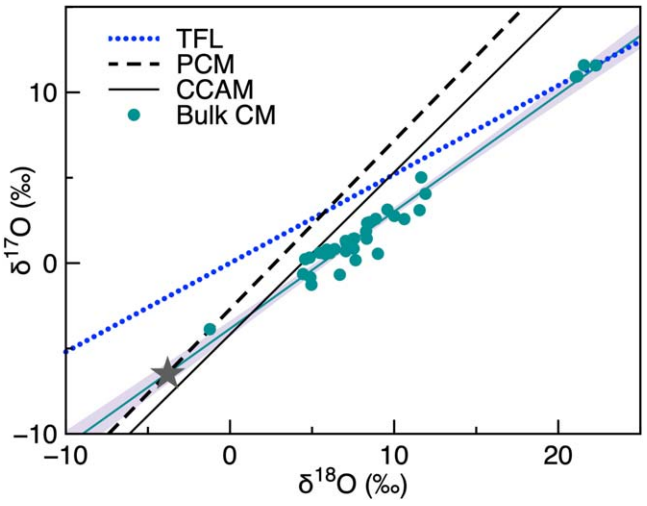

Figure 6. $\delta^{17}O$–$\delta^{18}O$ plot showing the O isotopic composition of the anhydrous CM protolith (i.e., the theoretical anhydrous bulk CM composition: $\delta^{18}O = -3.8‰$ and $\delta^{17}O = -6.5‰$; gray star) determined from the linear correlation of the CM bulk composition (green circle; Clayton & Mayeda 1999; Hewins et al. 2014). The anhydrous CM protolith corresponds to the intercept between the bulk CM trend ($\delta^{17}O = 0.69 \times \delta^{18}O$–3.8; $n = 36$) and the PCM line ($\delta^{17}O = 0.987 \times \delta^{18}O$–2.7; Ushikubo et al. 2012). CCAM = Carbonaceous chondrite anhydrous minerals line.

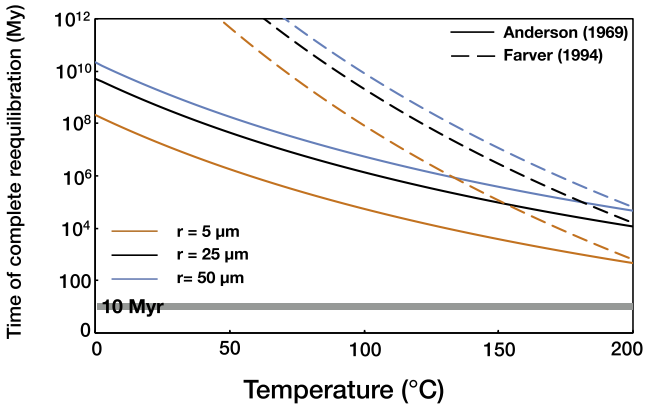

Figure 7. Time (Myr) required for the complete re-equilibration of early precipitated T1 calcite as a function of grain size (radius) and temperature, calculated using oxygen self-diffusion parameters for calcite (Farver 1994). The gray shaded region at 10 Myr corresponds to the duration estimated for fluid circulations in asteroidal parent bodies (Petitat et al. 2011; Fujiya et al. 2012; Doyle et al. 2015).

Table 3
Oxygen Isotopic Compositions of T2 Calcite Grains in the CM Chondrites Jbilet Winselwan and Mukundpura

#	$\delta^{18}O$	2σ	$\delta^{17}O$	2σ	$\Delta^{17}O$	2σ
CC15	17.1	0.4	8.1	0.9	−0.8	0.9
CC14	17.9	0.5	8	0.8	−1.3	0.0
Mean	17.5		8.1		−1	
StDev	*0.6*		*0*		*0.3*	
CC3-1	12.4	0.6	5.6	0.3	−0.9	0.5
CC3-4	12.5	0.6	4.3	0.4	−2.2	0.6
CC3-3	13	0.6	4.6	0.4	−2.2	0.6
CC3-2	15	0.5	6.5	0.4	−1.2	0.6
CC17-1	14.7	0.6	4.9	0.4	−2.7	0.6
CC17-2	17.7	0.6	6.1	0.4	−3.1	0.6
CC5-1	14.8	0.7	5.6	0.4	−2	0.6
CC5-5	15	0.8	4.2	0.5	−3.6	0.7
CC5-3	15.8	0.7	4.6	0.4	−3.6	0.7
CC5-2	16.6	0.5	4.7	0.4	−3.9	0.5
CC5-4	16.7	0.6	4.7	0.5	−4	0.6
CC6-1	17.2	0.6	6.5	0.4	−2.5	0.6
CC9	18.6	0.8	7.3	0.4	−2.4	0.7
Mean	15.4		5.4		−2.6	
StDev	*2.0*		*1.0*		*1.0*	

Note. Shaded rows denote multiple analyses of the same grain.

ORCID iDs

Lionel G. Vacher https://orcid.org/0000-0003-4230-6748
Yves Marrocchi https://orcid.org/0000-0001-7075-3698

References

Alexander, C. M. O'd, Bowden, R., Fogel, M. L., & Howard, K. T. 2015, M&PS, 50, 810
Anderson, T. F. 1969, JGR, 74, 3918
Benedix, G. K., Leshin, L. A., Farquhar, J., et al. 2003, GeCoA, 67, 1577
Bonal, L., Bourot-Denise, M., Quirico, E., et al. 2007, GeCoA, 71, 1605
Brearley, A. J. 2006, MESS II, 943, 587
Briani, G., Gounelle, M., Bourot-Denise, M., & Zolensky, M. E. 2012, M&PS, 47, 880
Burbine, T., McCoy, T., Meibom, A., Gladman, B., & Keil, K. 2002, in Asteroids III, Vol. 1, ed. W. F. Bottke, Jr. et al. (Tucson, AZ: Univ. Arizona Press), 653
Busemann, H., Alexander, C. M. O'D., & Nittler, L. R. 2007, M&PS, 42, 1387
Clayton, R. N., & Mayeda, T. K. 1984, EPSL, 67, 151
Clayton, R. N., & Mayeda, T. K. 1999, GeCoA, 63, 2089
Cody, G. D., Alexander, C. M. O'D., Yabuta, H., et al. 2008, EPSL, 272, 446
Doyle, P. M., Jogo, K., Nagashima, K., et al. 2015, NatCo, 6, 7444
Farver, J. R. 1994, EPSL, 121, 575
Früh-Green, G. L., Plas, A., & Lécuyer, C. 1996, 14. Proc. Ocean Drilling. Programm., 147, 255
Fuchs, L. H., Olsen, E., & Jensen, K. J. 1973, Smithsonian Contr. Earth Sci., 10, 1
Fujiya, W. 2018, EPSL, 481, 264
Fujiya, W., Sugiura, N., Hotta, H., et al. 2012, NatCo, 3, 627
Fujiya, W., Sugiura, N., Marrocchi, Y., et al. 2015, GeCoA, 161, 101
Ganino, C., & Libourel, G. 2017, NatCo, 8, 261
Ghosh, P., Adkins, J., Affek, H., et al. 2006, GeCoA, 70, 1439
Guo, W., & Eiler, J. M. 2007, GeCoA, 71, 5565
Hamilton, V. E., Simon, A. A., Christensen, P. R., et al. 2019, NatAs, 3, 332
Hewins, R. H., Bourot-Denise, M., Zanda, B., et al. 2014, GeCoA, 124, 190
Hiroi, T., Zolensky, M. E., Pieters, C. M., & Lipschutz, M. E. 1996, M&PS, 31, 321
Howard, K. T., Benedix, G. K., Bland, P. A., & Cressey, G. 2009, GeCoA, 73, 4576
Howard, K. T., Benedix, G. K., Bland, P. A., & Cressey, G. 2011, GeCoA, 75, 2735
King, A. J., Russell, S. S., Schofield, P. F., et al. 2018, M&PS, 54, 521
Kitazato, K., Milliken, R. E., Iwata, T., et al. 2019, Sci, 364, 272
Lauretta, D. S., DellaGiustina, D. N., Bennett, C. A., et al. 2019, Natur, 568, 55
Lee, M. R., Lindgren, P., & Sofe, M. R. 2014, GeCoA, 144, 126
Lee, M. R., Sofe, M. R., Lindgren, P., Starkey, N. A., & Franchi, I. A. 2013, GeCoA, 121, 452
Lindgren, P., Lee, M. R., Starkey, N. A., & Franchi, I. A. 2017, GeCoA, 204, 240
Marrocchi, Y., Bekaert, D. V., & Piani, L. 2018, EPSL, 482, 23
Marrocchi, Y., Gounelle, M., Blanchard, I., et al. 2014, M&PS, 49, 1232
O'Neil, J. R., Clayton, R. N., & Mayeda, T. K. 1969, JChPh, 51, 5547
Petitat, M., Marrocchi, Y., McKeegan, K. D., et al. 2011, M&PS, 46, 275
Piani, L., Yurimoto, H., & Remusat, L. 2018, NatAs, 2, 317
Pignatelli, I., Marrocchi, Y., Mugnaioli, E., et al. 2017, GeCoA, 209, 106
Pignatelli, I., Marrocchi, Y., Vacher, L. G., et al. 2016, M&PS, 51, 785
Rubin, A. E., Trigo-Rodriguez, J. M., & Huber, H. 2007, GeCoA, 71, 2361
Rudraswami, N. G., Naik, A. K., Tripathi, R. P., et al. 2018, Geosci. Front., 10, 495
Sakamoto, N., Seto, Y., Itoh, S., et al. 2007, Sci, 317, 231
Sugita, S., Tatsumi, E., Okada, T., et al. 2019, Sci, 364, 252
Sugiura, N., & Fujiya, W. 2014, M&PS, 49, 772
Ushikubo, T., Kimura, M., Kita, N. T., & Valley, J. W. 2012, GeCoA, 90, 242
Vacher, L. G., Marrocchi, Y., Verdier-Paoletti, M. J., Villeneuve, J., & Gounelle, M. 2016, ApJL, 827, L1
Vacher, L. G., Marrocchi, Y., Villeneuve, J., Verdier-Paoletti, M. J., & Gounelle, M. 2017, GeCoA, 213, 271
Vacher, L. G., Marrocchi, Y., Villeneuve, J., Verdier-Paoletti, M. J., & Gounelle, M. 2018, GeCoA, 239, 213
Vacher, L. G., Truche, L., Faure, F., et al. 2019, M&PS, 54, 1870
van Kooten, E. M. M. E., Cavalcante, L. L., Nagashima, K., et al. 2018, GeCoA, 79, 102
Verdier-Paoletti, M. J., Marrocchi, Y., Avice, G., et al. 2017, EPSL, 458, 273
Vilas, F. 1994, Icar, 111, 456
Vilas, F., & Gaffey, M. J. 1989, Sci, 246, 790
Watanabe, S., Hirabayashi, M., Hirata, N., et al. 2019, Sci, 364, 26
Watkins, J. M., Nielsen, L. C., Ryerson, F. J., & DePaolo, D. J. 2013, EPSL, 375, 349
Young, E. D., Zhang, K. K., & Schubert, G. 2003, EPSL, 213, 249
Zheng, Y.-F. 1993, GeCoA, 57, 1079
Zolensky, M. E., Mittlefehldt, D. W., Lipschutz, M. E., et al. 1997, GeCoA, 61, 5099